This is a repository copy of *Slipcasting of MAX phase tubes for nuclear fuel cladding applications*.

White Rose Research Online URL for this paper:
http://eprints.whiterose.ac.uk/156786/

Version: Published Version

Article:

Slipcasting of MAX phase tubes for nuclear fuel cladding applications

T. Galvin[a,*], N.C. Hyatt[a], W.M. Rainforth[a], I.M. Reaney[a], D. Shepherd[b]

[a] Department of Materials Science and Engineering, University of Sheffield, Sir Robert Hadfield Building, Mappin St, Sheffield S1 3JD, UK
[b] National Nuclear Laboratory (NNL), NNL Preston Laboratory, Springfields, Preston PR4 0XJ, UK

ABSTRACT

As a proof of concept, tubes of Ti_3SiC_2 MAX phase were slipcast in order to investigate its potential for the fabrication of fuel cladding for nuclear reactors. A slip consisting of 46% dry weight basis (dwb) water, 4% dwb polyethyleneimine (PEI), 0.5% dwb methylcellulose was used to cast the tubes, which were then sintered for 2 h under vacuum at 1450 °C. Silicon loss was observed at surface which resulted in the formation of TiC. The hoop stress to destruction of the tubes was measured and achieved a maximum of 9.1 $\pm$ 2.2 MPa/mm of tube thickness.

1. Introduction

Originally discovered in the 1960s [1], the family of layered ternary nitrides and carbides known as $M_{n+1}AX_n$ phases have been heavily researched since the discovery of their unusual combination of properties in the 1990s by Barsoum and El-Raghy [2]. They are formed from a transition metal element (M), a metalloid element (A) and carbon or nitrogen (X) and have the crystallographic space group P6$_3$/mmc. Over 150 different compositions have now been synthesised, with the majority of these having been discovered in the past few years [3]. Exhibiting traits of both metals (high electrical and thermal conductivity and reasonable fracture toughness) and ceramics (high temperature strength and creep resistance) [4], they currently find use in high temperature applications such as heating elements, furnace tubes and burner nozzles [5].

Some MAX phases form a protective oxide scale upon heating in air which protects the bulk from further oxidation [6]. They also show excellent corrosion resistance in heavy liquid metals (HLM), with Ti_3SiC_2 being an example of a successful phase in liquid sodium [7] and liquid lead-based systems, in the latter this includes the commercially available impure MAXTHAL® 312 grade from Sandvik Kanthal reported to contain ~10 wt.% Ti [8–10]. These are the respective coolants for sodium- and lead-cooled fast reactor designs (SFR and LFR). Fast reactors have the potential to be much more sustainable than current thermal (slow) neutron nuclear systems e.g., pressurised water reactors (PWR). This is because fast reactors are capable of breeding a net gain of fresh fissile plutonium from depleted uranium allowing nuclear fuel to be recycled many times, and they also generate negligible very long-lived nuclear waste (minor actinides) and are even capable of transmuting stockpiles of these elements produced in thermal reactors.

Neutron and proton irradiation studies on select MAX phases performed by Tallman et al. [11,12] and Ward et al. [13] respectively, conclude that some phases (Ti_3SiC_2 and Ti_3AlC_2) have some resistance to amorphisation during irradiation at PWR temperatures (~350 °C) however dissociation to TiC was seen. They are more promising at the higher irradiation temperatures (greater than ~500 °C) typical of fast reactors and may exhibit dynamic recovery at higher temperatures (>695 °C).

The overall combination of properties has led to MAX phases being proposed as a candidate for nuclear fuel cladding applications including LFR and in accident tolerant fuel (ATF) for PWRs, as well as impellers for LFRs [9,14]. Although, it should be noted that none of the currently synthesised phases has yet been shown to be suitable for an ATF application. While Cr_2AlC has shown good corrosion resistance in PWR water chemistry [15], its irradiation resistance has so far been found to be unsuitable [16]. Cladding must also be of sufficiently low neutron absorption and activation for its reactor application, with the requirement for ATF being much more challenging as the neutronics of currently used zirconium alloys are highly favourable [17]. A number of Zr-based MAX phases have now been synthesised [3] but the corrosion and irradiation resistance of phases tested so far has been insufficient [9,18] as was the apparent mechanical strength [17] which dictates required clad thickness and hence neutronic suitability. However, novel Zr-based MAX continue to be synthesised and so it remains possible that a suitable phase will be identified.

Furthermore, before MAX phases can be considered for a cladding application, the ability to form them into the required long thin tube geometry must be explored. There are several possible options to create

* Corresponding author.
  E-mail address: TomGalvin@mimaterials.com (T. Galvin).

tube structures for ceramics. These include extrusion [5,19] and 3D printing [20]. It is tempting, given the novel nature of MAX phases, to apply a 'high tech' solution to this challenge. However, slipcasting is a traditional process that is widely used in ceramic technology e.g., for the fabrication of sinks, toilets and decorative pottery. Although not frequently utilised for technical ceramics, slipcasting of Ti_2AlC MAX phase components has been demonstrated by Sun et al. [21], while Hu et al. slip cast highly oriented Nb_4AlC_3 in a magnetic field which they densified using Spark Plasma Sintering (SPS) [22]. Moreover, Barsoum and El-Raghy reported that Ti_3SiC_2 may be cast to complex geometries for the manufacture of non-stick moulds for latex gloves and condom formers [4,23]. The use of slipcasting has also been shown to be able produce complex shapes from MAX phases [5]. In this paper, we therefore explore the possibility of producing tubes from MAX phases via slipcasting.

2. Materials and methods

Commercial Ti_3SiC_2 (MAXTHAL® 312) was used as substituent for a potential reactor-suitable MAX phase cladding composition to demonstrate proof of concept. The powder contained approximately 15 wt%. of TiC impurity. It should be noted that Ti_3SiC_2 would be unsuitable for ATF applications due its poor oxidation resistance at high temperatures [24], though its potential application in LFR cladding is more promising as discussed in the Introduction. The particle size of the feedstock power is shown in Fig. 1. Particle size data was collected on a Malvern Mastersizer 2000 with the powder dispersed in water at 2.75% obscuration. Mie scattering analysis was used, with an absorption value of 1 and a refractive index estimated from Ali et al. [25]. The powder/ water suspension was ultrasonicated between data collection runs to break up agglomerates. The powder was found to have a mass median diameter of 7.07 + 0.30 μm.

2.1. Slipcasting

2.1.1. Slip formation

PEI (Sigma Aldrich, molecular weight (M_w) 25,000, <1% water) was used as dispersant in the slip, while methylcellulose (Sigma Aldrich, viscosity of 4000 centiPoise (cP)) was used as a thickener to increase the viscosity without further raising the solids loading. Moulds were fabricated from Plaster of Paris (JW Superwhite) according to the

Table 1
Composition of the slips used for rheological testing.

x	Water (%dwb)	PEI (%dwb)	Methylcellulose (%dwb)
A	46.0	4.0	0.0
B	46.0	4.0	0.5
C	46.0	4.0	1.0
D	50.0	4.0	0.0
E	50.0	4.0	0.5
F	50.0	4.0	1.0
G	52.0	4.0	0.0
H	52.0	4.0	0.5
J	52.0	4.0	1.0

manufacturer's instructions with modelling clay used to create a seal, and washing-up liquid to act as mould release.

Methylcellulose is hygroscopic and prone to clumping when added to water. However, it has the unusual property of being insoluble in hot water (>50 °C) while having a high solubility in cold water which, along with the high viscosity and strand forming tendency of PEI, led to the following procedure being used for slip preparation. To ensure proper dispersion, PEI was weighed into a beaker to which the appropriate volume of water was added to correspond to the correct H_2O : PEI ratio to give the concentrations specified in Table 1. The solution was placed on a hotplate (Jenway 1000) set at 70 °C while being intermittently stirred with a glass rod, until the strands of PEI had completely dissolved, after which the beaker was removed from the hotplate (while still only lukewarm i.e., <70 °C to minimise losses of H_2O through evaporation). The methylcellulose was weighed and quickly added to the beaker. The Ti_3SiC_2 powder (Maxthal® 312, Sandvik Kanthal which was measured by XRD to contain 10–15 vol.% TiC impurity and a median particle size of 7.07 ± 0.30 μm by low angle laser scattering) was weighed and added with additional stirring. The warm slip was transferred to an Azlon mill bottle (250 ml) and the samples were roller milled as they cooled at 30 rpm (Brook Crompton TYP T-DA63MB-D).

2.1.2. Rheology

An initial slip was created using 50% dwb of water, and 2.5% dwb PEI (equivalent to 40:20:1 MAX phase:water:PEI). This slip was not degassed prior to casting and produced a poor green body strength with many large air inclusions. Subsequent slips were de-gassed (see below),
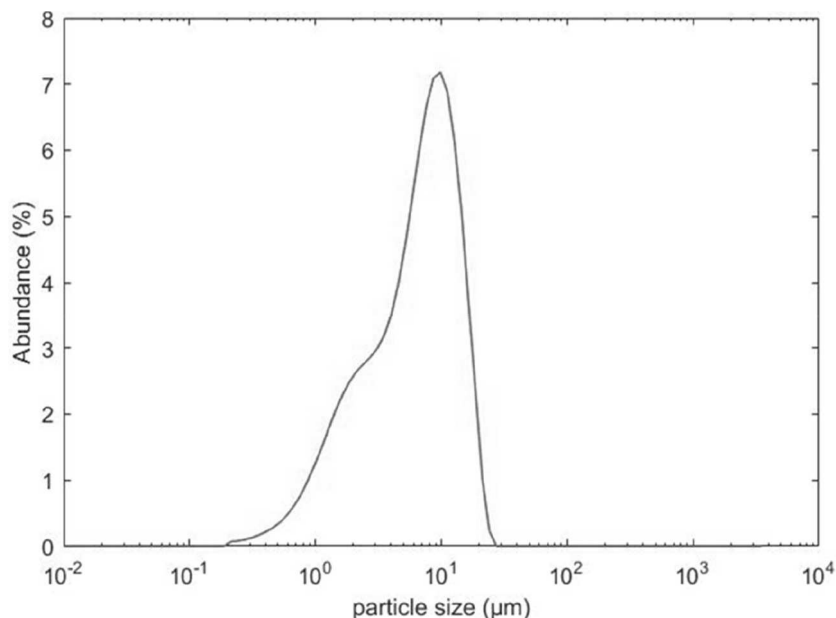

Fig. 1. Particle size analysis data for MATHAL312 powder feedstock.

and a more thorough investigation of slip composition carried out. The de-gassing process was required to remove the many bubble inclusions in the slip after mixing, and involved placing the slip container in a vacuum chamber and pulling a vacuum for 5 min, then rapidly restoring atmospheric pressure.

Small batches of slips were prepared and kept agitated on a tube roller (Cole Palmer) at 30 rpm with varying water and methylcellulose content, displayed in Table 1. All percentages are given as a fraction by weight of the Ti_3SiC_2 used (dwb). The samples were tested using an AR2000 rheometer (TA instruments), using cone and plate geometry (40 mm diameter, 2° angle, 55 μm truncation) at 25 °C. A pre-shear phase with constant shear rate of 1 s^{-1} was applied for each sample for 120 s. This was performed largely to ensure the sample was well distributed between the plates, and to check there were no large agglomerates or air bubbles. The shear rate was then increased logarithmically between 0 and 100 s^{-1} with 10 s on each of 16 steps.

2.1.3. Mould preparation and casting

A mould was made to approximately the radial dimensions of a fuel cladding rod. The mould former was 11.5 mm in diameter, 15 cm in length with a rounded bottom edge to facilitate easier removal. The former was used to make both a one and a two piece mould, and was designed in FreeCAD v0.15 software and then reproduced in polished brass (Fig. 2). The two piece mould was made with three keying features to ensure the halves were aligned correctly. Immediately prior to casting, slips were de-gassed to remove bubbles by placing the open mill bottle in a vacuum desiccator and evacuating for 5 min (KNFlabs N86KT.18 pump, 160 mbar) and then quickly restoring atmospheric pressure by removal of the hose.

The slip was poured into the mould and left for 2 min (topping up the slip level if needed), whereupon the excess slip was poured from the mould and the resulting cast left to drain and dry for 2 weeks before demoulding was attempted. We note that drying periods in the ceramics industry are typically much shorter in optimised processes (~24 h) but longer times were used at this proof of concept stage to minimise the risk cracking on removal.

2.2. Sintering

Green parts were sintered following a two-step process. Polymers and organics were removed from the slip by heating for 1 h at 500 °C. This was followed by sintering for 2 h with temperatures trialled between 1300 and 1450 °C in a tube furnace under flowing argon (Carbolite STF 15/75/450, ~0.25 L/min) or vacuum (Elite TSF15-50/180-2416 with Edwards RV3 pump, $2\,2 \times 10^{-3}$ mbar ultimate pressure). Both furnaces were atmosphere-controlled tube furnaces, with heating elements external to the alumina tubes.

2.3. Characterisation

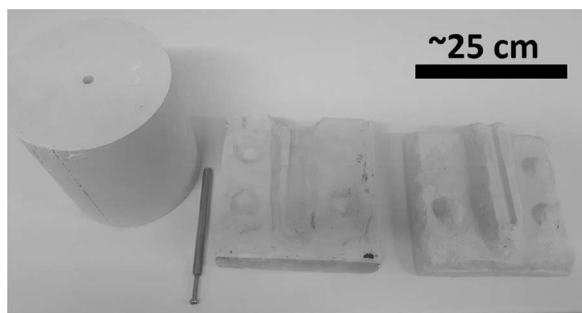Density measurements were performed using a helium pycnometer

and the Archimedes method with water (immersion density). Samples often contained open porosity so density/porosity measurements were also undertaken using ImageJ software (Version 1.51 u, National Institute of Health). Densified samples were sectioned (Buehler Isomet), polished and examined using a Hitachi TM3030 scanning electron microscope (SEM) equipped with energy dispersive x-ray (EDX) spectroscopy (Bruker Quantax 70). Samples were ground using P260 and P600 diamond grinding discs (MetPrep Cameo Platinum series) using water lubrication. Polishing was carried out using a 3 μm Apex Diamond Grinding disc (Buehler) and 1 μm water-based diamond suspensions (MetPrep monocrystalline) on cashmere polishing cloth (MetPrep). Fracture surfaces after hoop strength testing were also examined by SEM. X-ray diffraction (XRD) was performed on a Bruker D2 Phaser from 10° ≤ 2θ ≤ 70° and a 0.02° step size using a Cu kα source.

2.4. Finishing and hoop strength testing

Sintered tubes were drilled out to an internal diameter of 6 mm using a tool steel bit in a pillar drill. The tubes were hand polished using SiC papers to ensure an even wall thickness which was checked with a calliper. P200 paper was used initially, and subsequently P600, P1200 and P1800. Tubes were covered in the paper and ground with a combination of axial and rotational motion by hand. Sections that deviated from the proscribed thickness were excluded from testing, along with any bevelled or damaged pieces. 6 mm long sections were cut from the tubes and tested on a bespoke hoop stress rig (modelled in FreeCad v0.15) simplified from other designs in the literature [26–28]. The rig (Fig. 3) compresses a polyurethane bung uniaxially within the tube section, which exerts radial force on the inside face of the tube until it fractures, thus simulating increasing internal pressure in a sealed system such as increasing fission gas pressure in a clad tube. Lamé's equation was used to determine the maximum hoop stress σ_θ (Eq. (1)). Thin wall approximations were not valid for the tested tube dimensions (the thickness was greater than a tenth of the radius), and so hoop stress would vary non-negligibly through the thickness as a function of the radius.

$$\sigma_\theta = \frac{r_i^2 P_i - r_o^2 P_o}{(r_o^2 - r_i^2)} + \frac{(P_i - P_o) r_i^2 r_o^2}{(r_o^2 - r_i^2) r^2} \tag{1}$$

where: P_i and P_o are the internal and external pressure (atmospheric) respectively, r_i and r_o are the internal and external radii of the tube, and r is the radius at a given point through the thickness.

3. Results

3.1. Slip rheology

The viscosity of the slips with increasing shear rate is shown in Fig. 4, along with values displayed at a shear rate of 10 s^{-1}. Slips without methylcellulose behaved approximately as Newtonian fluids (viscosity independent of shear rate), with decreasing water content
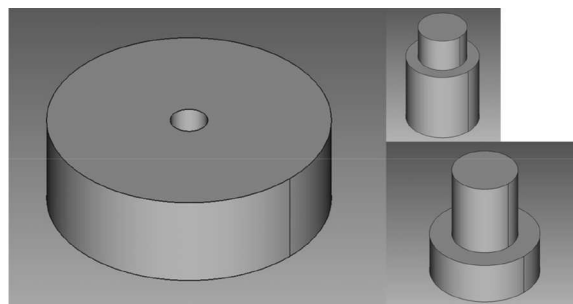

Fig. 2. Brass mould former shown with a one piece and a two piece plaster mould.

Fig. 3. (Clockwise from left) CAD models of the steel baseplate, polyurethane bung with aligning pin, and steel press ram.
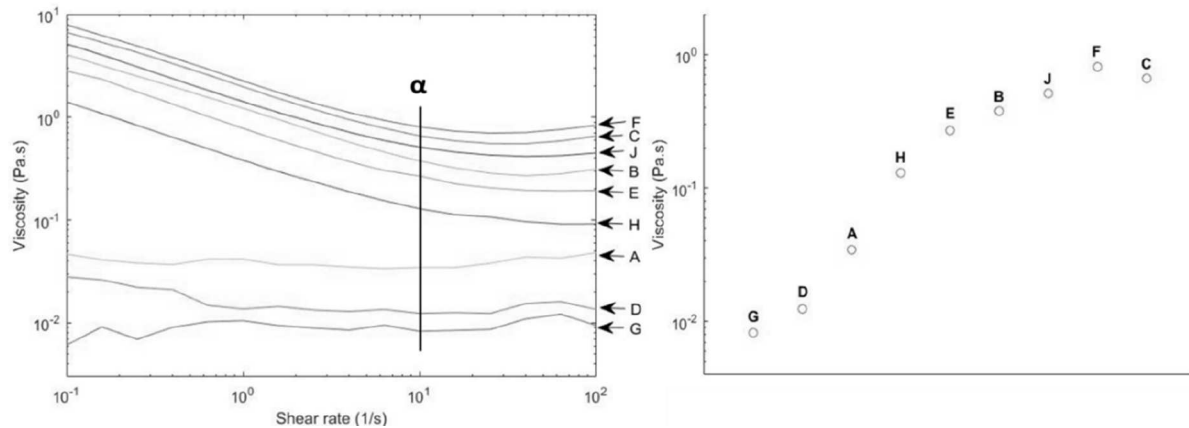
Fig. 4. Viscosity of slips with increasing shear rate (left), Viscosities at point α (10 s^{-1}) displayed in expected increasing viscosity (based on quantity of additives).

increasing the viscosity. The addition of methylcellulose resulted in shear-thinning (decreasing in viscosity with applied shear strain), as well as an increase in viscosity compared to the samples with only PEI. Viscosity increased with decreasing water content but slip C with 46% dwb water, which was expected to be the most viscous, was actually less viscous than slip F with 50% dwb water, possibly due to the hygroscopic and hydrophilic nature of methylcellulose [29]. There was a higher degree of variation in the shear-viscosity curves for samples with no methylcellulose. This could be due to a poor suspension, or agglomerations. This was not seen in methylcellulose containing samples, so these were chosen. Slips J, F, and C were too viscous to pour easily, so slip B (46% dwb water, 4% dwb PEI, 0.5% dwb MC) was selected to use for further experiments.

3.2. Sintering

Samples sintered in argon were very weak and powdery after heating, with little consolidation taking place but samples sintered under vacuum at 1400 and 1450 °C did densify. TiO_2 was also observed in samples sintered under argon; this is attributed to incomplete purging of the furnace, or an issue with the sealing of the tube. XRD traces are shown in Fig. 5. The starting powder contained some TiC, however, the intensity of TiC peaks increased after sintering, suggesting partial decomposition of the Ti_3SiC_2.

SEM and EDX spectra mapping was used to characterise cross-sections cut from the tube. A tube made without de-gassing showed bubble inclusions (Fig. 6) and EDX maps revealed a Si deficient layer at the edge, which was also observed on the inner surface of the tube. Preferential loss of the 'A' element occurs in MAX phase thermal breakdown, due to its weaker bonding, and impurities in the material can lower the temperature at which this occurs [4]. We note that the outer region can be removed by grinding due to the excellent machinability of MAX phases and so does not represent a barrier to exploitation as cladding which is typically ground to ensure a smooth surface finish. ImageJ density estimates of tubes sintered at 1450 °C under vacuum for 2 h gave values equivalent to ~89% of theoretical density. Fig. 7 shows the tube microstructure and open porosity. Fig. 8 shows examples of cast tubes at various points during processing. Some samples had off-centre holes due to uneven bulk thickness of the plaster mould. Some longer tubes sagged and bent during sintering, so smaller straight sections were cut from these. After drilling and hand-grinding, the resulting tubes are shown in Fig. 9. Great care was taken to ensure even wall thickness while grinding. Despite de-gassing, some minor pits and bubbles were still visible at the surface.

3.3. Hoop strength tests

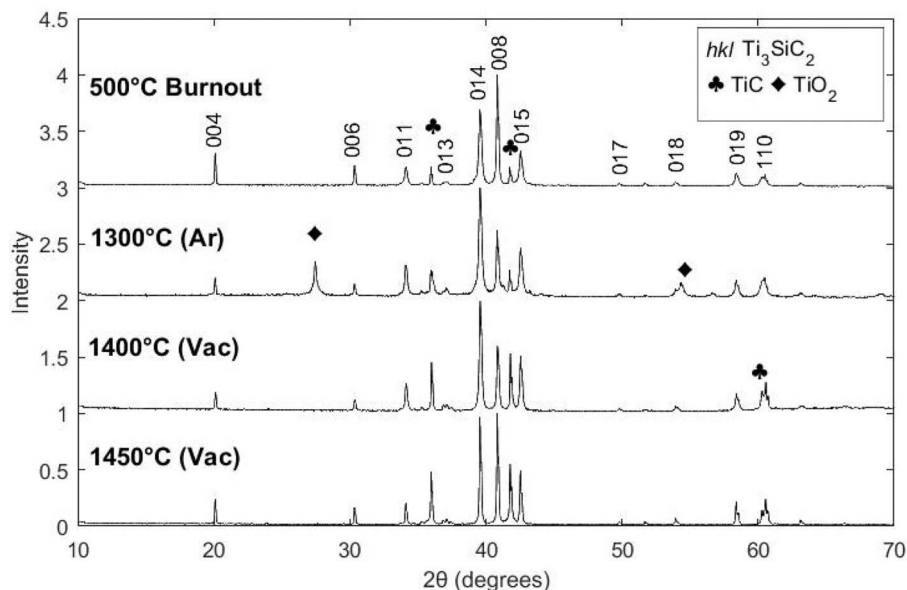Hoop strength tests were performed on tubes (labelled 1–6) sintered

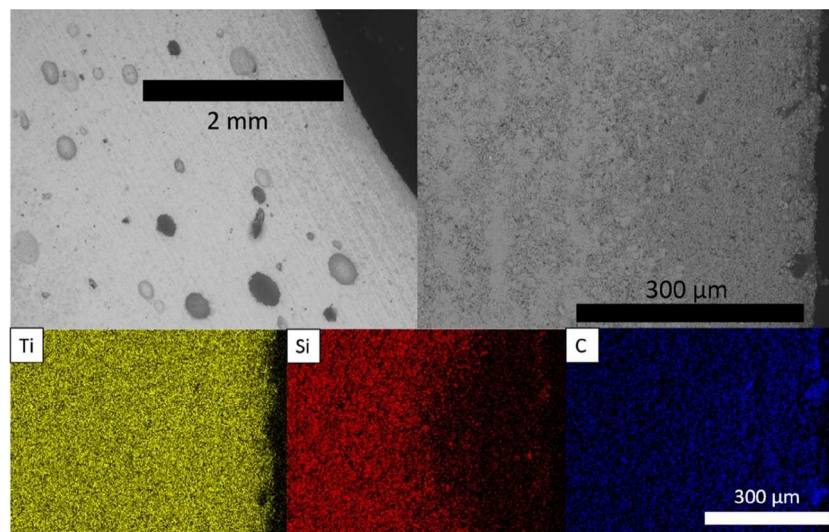**Fig. 5.** XRD data for samples sintered under different conditions.

Fig. 6. SEM images of a tube cross-section, showing bubble inclusions (top left), and the edge (top right). EDX spectra maps of the tube edge showing loss of silicon at the surface.

at 1450 °C under vacuum. Lame's equations for thick walled tubes give results that vary throughout the bulk, but values displayed in Fig. 10 show the maximum hoop stress (at the internal surface) for the tested tubes. There is significant variation for samples of similar wall thickness (all with the same process route), likely due to variation in internal defects and bubbles (see below). Table 2 shows the data gathered from the hoop strengths tests. Tube 4 gave the best value of maximum hoop stress per unit thickness (9.1 ± 2.2 MPa/mm). Uncertainty was conservatively estimated as $\pm 20\%$, for which further details are given in [30].

SEM images of the fracture surfaces are shown in Fig. 11. They reveal regions with small bubbles ~100 μm across, as well as grain pull-out. Tube 4 had large fissures on its fracture surface which most likely appeared post testing.

4. Discussion

The PEI only slips exhibited more variation in their rheology than those that containing methylcellulose. The addition of methylcellulose appeared to improve the rheological characteristics of the slurry and resulted in a shear-thinning which was beneficial as lower viscosity during pouring permits better permeation within the mould. Moreover, thickening within the mould slows the uptake of water resulting in a more uniform deposition. The de-gassing procedure significantly improved the open porosity of the casts. Many tubes however, had offset central holes after casting and required careful drilling. This was due to mould design in which one side was marginally thicker than the other, and so had more capacity for water uptake. These issues could most likely be resolved with future work if the technology was deemed promising for the fabrication of cladding. The sintered densities of the tubes were too low to be hermetically sealed, and in future a feedstock with smaller average particle size should be used to improve the density.

It should be noted again that in future iterations of slipcast tube fabrication, machine lathing can be used to remove the TiC layer, as discussed by Hwang et al. [31]. It is hoped that the relative thinness and
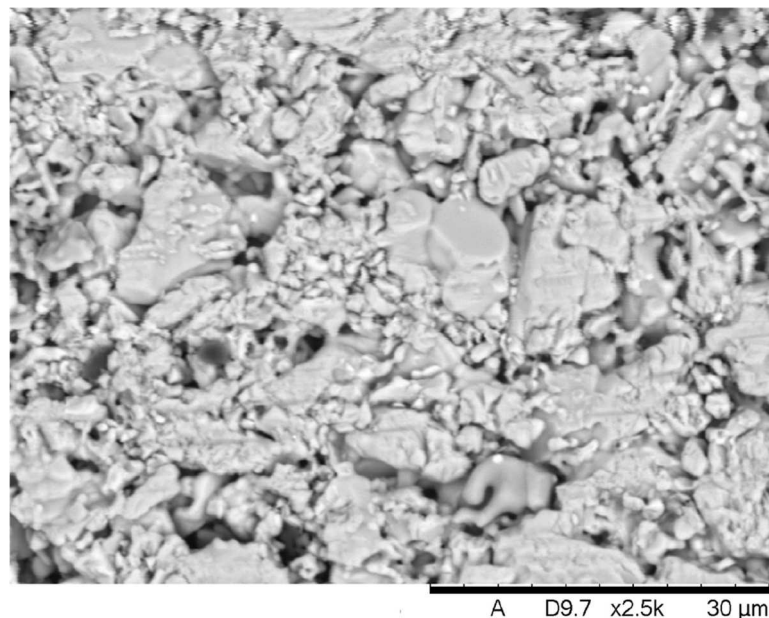

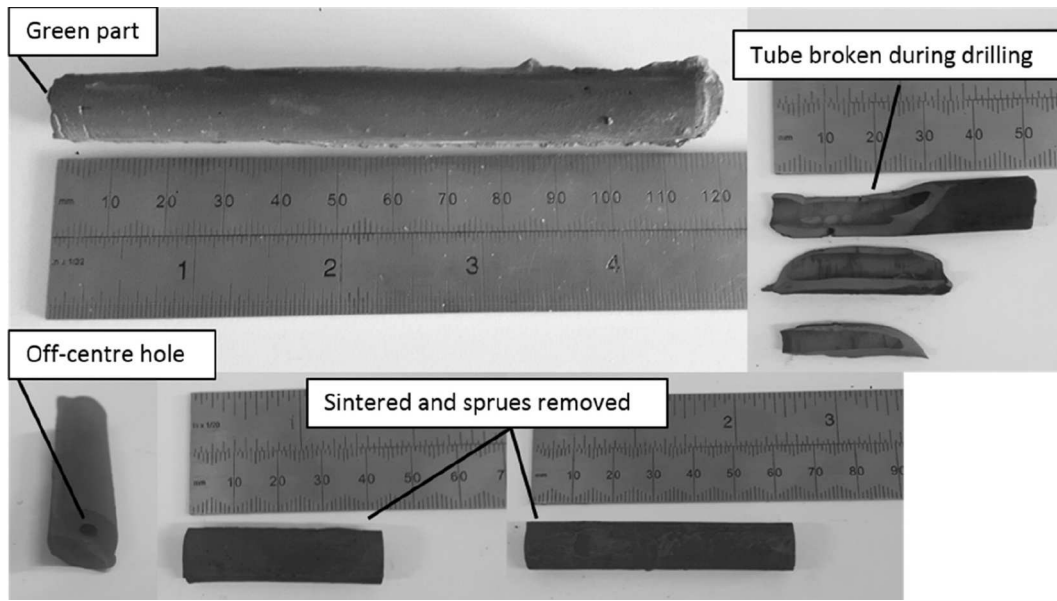**Fig. 7.** SEM images of sintered microstructure, showing porosity.

Fig. 8. Cast tubes at various stages during sintering and finishing.

low density of the binary carbide layer will ease removal; however the higher density tubes required for the application may present more of a problem.

There was a wide variation in the maximum hoop stresses, with no apparent correlation between wall thickness and failure stress, indicating a high degree of inconsistency in the manufacturing process. Porosity is visible in the fracture surfaces in Fig. 10 and most likely constituted flaws at which cracks initiated. Hairline cracks may also have been introduced through grinding, drilling and sectioning. Elimination of such strength-limiting flaws is critical for any future fabrication process.

Tube 4 had a wall thickness of 2.66 mm and reached a maximum hoop stress at the internal surface of 20.95 ± 4.19 MPa, giving a maximum hoop stress to wall thickness ratio of 9.07 ± 2.16 MPa/mm, which was the highest value for those tested. However, the required hoop strengths are far larger in current nuclear fuel clads.

In respect of a possible ATF application, then maximum hoop stress values have measured in literature by biaxial liquid pressure burst test in unirradiated (oxidation and hydrogen embrittlement excluded) Zr–1%Nb VVER cladding (Russian PWR equivalent) as ~950 MPa (~1350 MPa/mm) at ambient temperature, ~650 MPa at operational temperatures (~950 MPa/mm) and ~200 MPa (~300 MPa/mm) at
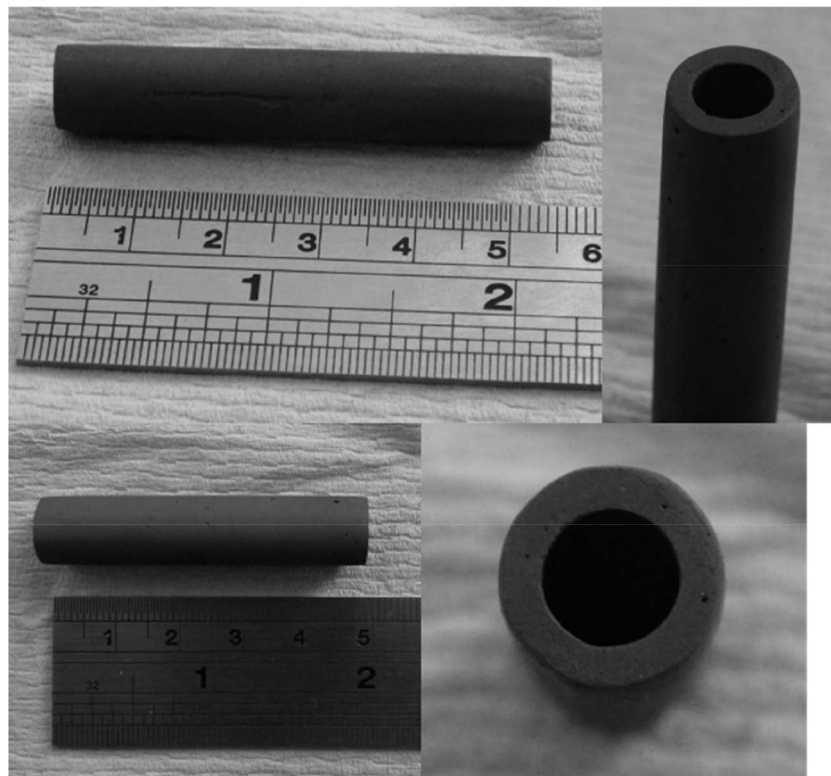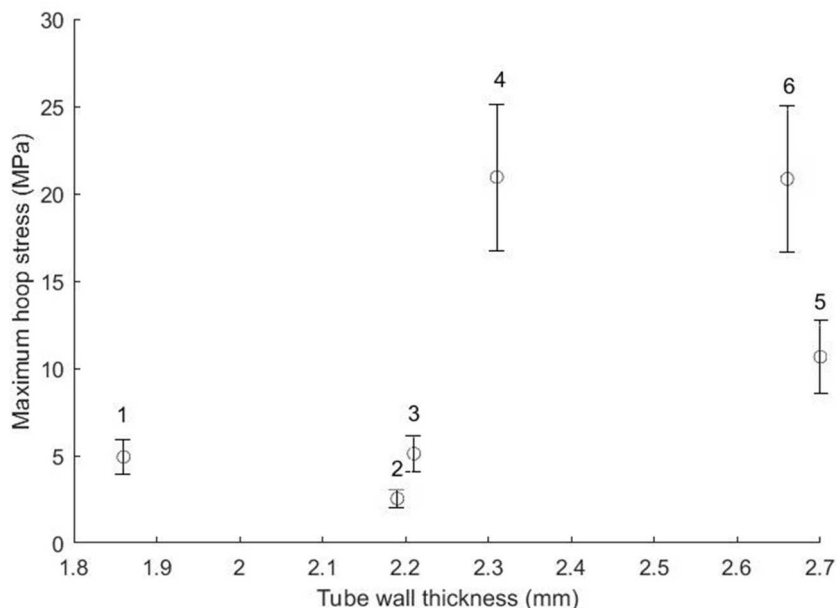

Fig. 9. Finished tube samples.

Fig. 10. Hoop stress maximum values (internal surface) of tested tubes. Bars represent a conservatively estimated measurement uncertainty of ± 20%.

Table 2
Summary of hoop strength test results with measurement uncertainty values.

Sample	Wall thickness (mm)	Maximum hoop stress (MPa)	Max. hoop stress per thickness (MPa/mm)
1	1.9 ± 0.3	4.9 ± 1	2.7 ± 0.8
2	2.2 ± 0.3	2.6 ± 0.5	1.2 ± 0.3
3	2.2 ± 0.2	5.1 ± 1.0	2.3 ± 0.6
4	2.3 ± 0.2	21.0 ± 4.2	9.0 ± 2.2
5	2.7 ± 0.2	10.7 ± 2.1	4.0 ± 0.8
6	2.7 ± 0.2	20.9 ± 4.2	7.9 ± 1.7

Fig. 11. Fracture surfaces of tube 1 and 4. Images oriented so tube radius is vertical.

~700 °C, although the value is almost nothing at ~1000 °C [32]. It should be noted that significantly variability has been reported between the maximum hoop stress values recorded for zirconium cladding alloys by different testing techniques including between liquid pressure burst tests and expansion due to compression (EDC) tests [33] as used in this paper.

For an SFR or LFR application, then the minimum hoop stress that must be withstood at operational temperatures of 480 – 550 °C should be anticipated to be in the range 100–150 MPa [34].

One factor that should be noted is Ti_3SiC_2 [35] and other MAX phases [36], unlike zirconium [32] and proposed fast reactor steel cladding alloys [36], do not lose significant strength below 1000 °C compared to ambient temperature values. However for this to be of benefit, then the strength of MAX phases at operational temperature must be competitive, taking into account the neutronically permissible thickness, i.e., significantly better than achieved in the present study.

In this regard, the thickness of the MAX phase tube able to be produced thus far by the method presented must also be considered – a wall thickness of 2.66 mm would not be feasible neutronically for current PWRs [17] (cladding thickness ~0.6 mm [38]) or fast reactors for which designs usually have even thinner clads [37,39], though typically of steels which have higher neutron absorption than zirconium cladding alloys.

Fabricating textured MAX phase tubes may provide way to improve the strength, and resist irradiation swelling. This could be achieved using a related technique called 'centrifugal slipcasting', where the mould is spun on its axis at a high rpm, while slip is fed into the mould through a coupler. This technique has been shown to preferentially orient platelet grains in the green body [41–43].

The work reported above nonetheless illustrated the potential for MAX phase tubes to be fabricated using slipcasting and was sufficiently successful to give confidence that further study would be able to address flaws and improve density, based on previous optimisation programmes undertaken using different materials. Using textured MAX phases or composites, similar to research being carried out with SiC/SiC fibre-reinforced material [40], could also provide a workable solution to improve the overall properties.

5. Conclusion

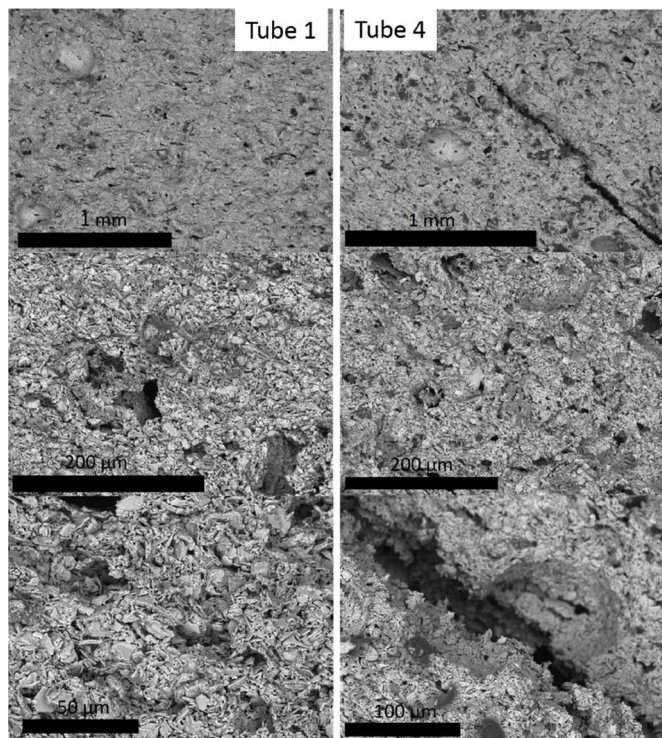Ti_3SiC_2 based slips containing PEI and methylcellulose were tested

for their rheological properties, and a slip containing 46% dwb water, 4% dwb PEI and 0.5% dwb methylcellulose was determined to have the most appropriate properties for slipcasting. Sintered slipcast tubes were 89% dense, with some silicon loss at the outer edges of the sintered part, which would be removable with grinding or machining. Destructive hoop strength tests at room temperature in atmospheric pressure were performed on hand finished sections, with the best result being 9.1 $\pm$ 2.2 MPa/mm of tube thickness. This value is too low to consider using as a cladding replacement at this juncture, but this work serves as further proof of concept that slipcasting can produce MAX phase tubes. Improvements in processing and densification would be expected to yield superior properties due to the elimination of internal flaws.

Data availability

The raw/processed data required to reproduce these findings cannot be shared at this time due to technical and time limitations.

Declaration of Competing Interest

The authors declare that they have no known competing financial interests or personal relationships that could have appeared to influence the work reported in this paper.

Acknowledgements

References

[1] W. Jeitschko, H. Nowotny, F. Benesovsky, Kohlenstoffhaltige ternaire verbindungen (H-Phase), Monatshefte für Chem. 332 (1963) 2–6.

[2] M.W. Barsoum, T. El-Raghy, Synthesis and characterization of a remarkable ceramic: Ti_3SiC_2, J. Am. Ceram. Soc. 79 (7) (1996) 1953–1956.

[3] M. Sokol, V. Natu, S. Kota, M.W. Barsoum, On the chemical diversity of the max phases, Trends Chem. 1 (2) (2019) 210–223, https://doi.org/10.1016/j.trechm.2019.02.016.

[4] M.W. Barsoum, MAX Phases: Properties of Machinable Ternary Carbides and Nitrides 1 Wiley-VCH, 2013.

[5] M. Ivermark, Presentation of Maxthal (Attended by D. Shepherd), Proceedings of the CARAT 2nd Annual Meeting, Manchester, 2014.

[6] M. Haftani, M. Saeedi Heydari, H.R. Baharvandi, N. Ehsani, Studying the oxidation of Ti_2AlC MAX phase in atmosphere: a review, Int. J. Refract. Met. Hard Mater. 61 (2016) 51–60.

[7] G.W. Bentzel, M. Ghidiu, J. Griggs, A. Lang, M.W. Barsoum, On the interactions of Ti_2AlC, Ti_3AlC_2, Ti_3SiC_2 and Cr_2AlC with pure sodium at 550°C and 750°C, Corros. Sci. 111 (2016) 568–573.

[8] L.A. Barnes, N.L. Dietz Rago, L. Leibowitz, Corrosion of ternary carbides by molten lead, J. Nucl. Mater. 373 (1–3) (2008) 424–428.

[9] K. Lambrinou, T. Lapauw, A. Jianu, A. Weisenberger, J. Ejenstam, P. Szak'los, et al., Corrosion-Resistant ternary carbides for use in heavy liquid metal coolants, Am. Ceram. Soc. 7 (2016) 19–34.

[10] T. Lapauw, B. Tunca, J. Joris, A. Jianu, R. Fetzer, A. Weisenberger, et al., Interaction of $M_{n+1}AX_n$ phases with oxygen-poor, static and fast-flowing liquid lead-bismuth eutectic, J. Nucl. Mater. 520 (2020) 258–272, https://doi.org/10.1016/j.jnucmat.2019.04.010.

[11] D.J. Tallman, L. He, B.L. Garcia-Diaz, E.N. Hoffman, G. Kohse, R.L. Sindelar, et al., Effect of neutron irradiation on select MAX phases, Acta Mater. 85 (2015) 132–143.

[12] D.J. Tallman, L. He, J. Gan, E.N. Caspi, E.N. Hoffman, M.W. Barsoum, Effect of neutron irradiation on defect evolution in Ti_3SiC_2 and Ti_2AlC, J. Nucl. Mater. 468 (2016) 194–206.

[13] J. Ward, S. Middleburgh, M. Topping, A. Garner, D. Stewart, M.W. Barsoum, et al., Crystallographic evolution of MAX phases in proton irradiating environments, J. Nucl. Mater. 502 (2018) 220–227.

[14] B. Tunca, T. Lapauw, O.M. Karakulina, M. Batuk, T. Cabioc'h, J. Hadermann, et al., Synthesis of MAX phases in the Zr-Ti-Al-C system, Inorg. Chem. 56 (6) (2017) 3489–3498.

[15] J. Ward, et al., Corrosion performance of Ti_3SiC_2, Ti_3AlC_2, Ti_2AlC and Cr_2AlC MAX phases in simulated primary water conditions, Corros. Sci. 139 (February) (2018) 444–453.

[16] J. Ward, "MAX Phase Ceramics for Nuclear Applications, Ph.D. Thesis, University of Manchester," 2018.

[17] C. Grove, D. Shepherd, M. Thomas, P. Little, Neutronics of MAX phase materials, Struct. Mater. Innov. Nucl. Syst. (SMINS-4), Univ. Manchester (2016).

[18] K. Lambrinou, Accelerated development of MAX phases for accident-tolerant fuels (ATFs) [Presentation], Adv. Accid. Radiat. Toler. Mater. (2019).

[19] F. Händle, Extrusion in Ceramics, Springer-Verlag, 2009.

[20] Z. Chen, Z. Li, J. Li, C. Liu, C. Lao, Y. Fu, et al., 3D printing of ceramics: a review, J. Eur. Ceram. Soc. 39 (2018) (2019) 661–687.

[21] Z. Sun, M. Li, L. Hu, X. Lu, Y. Zhou, Surface chemistry, dispersion behavior, and slip casting of Ti_3AlC_2 suspensions, J. Am. Ceram. Soc. 92 (8) (2009) 1695–1702.

[22] C. Hu, Y. Sakka, H. Tanaka, T. Nishimura, S. Grasso, Fabrication of textured Nb_4AlC_3 ceramic by slip casting in a strong magnetic field and spark plasma sintering, J. Am. Ceram. Soc. 94 (2) (2011) 410–415.

[23] T. El-Raghy and M.W. Barsoum, "Max Phase Glove and Condom Formers," US 2004/0250334 A1, 2004.

[24] Z Sun, Y Zhou, M Li, Oxidation behaviour of Ti_3SiC_2-based ceramic at 900–1300°C in air, Corros. Sci. 43 (6) (2001) 1095–1109.

[25] M.S. Ali, A.K.M.A. Islam, M.M. Hossain, F. Parvin, Phase stability, elastic, electronic, thermal and optical properties of $Ti_3Al_{1-x}Si_xC_2$ ($0 \leq x \leq 1$): first principle study, Phys. B Condens. Matter 407 (21) (2012) 4221–4228.

[26] K. Mosley, The stressing for test purposes of materials in tubular form using elastomeric inserts—experimental and theoretical development, Proc. Inst. Mech. Eng. 196 (1) (1982) 123–139.

[27] W.R. Hendrich, W.J. McAfee, and C.R. Luttrell, "Expanded Plug Method for Developing Circumferential Mechanical Properties of Tubular Materials," US 7140259 B2, 2006.

[28] H. Jiang and J.A.J. Wang, Methodology for Mechanical Property Testing of Fuel Cladding Using an Expanding Plug Wedge Test, vol. 446, no. 1–3. 2014.

[29] "Methyl cellulose." [Online]. Available: https://www.chemicalbook.com/ChemicalProductProperty_EN_CB3474718.htm. [Accessed: 18-Mar-2019].

[30] T. Galvin, "The Use of Max Phases in Accident Tolerant Fuel Cladding, Thesis, The University of Sheffield," 2018. Available: http://etheses.whiterose.ac.uk/id/eprint/23258.

[31] S. Hwang, S.C. Lee, J. Han, D. Lee, S. Park, Machinability of Ti_3SiC_2 with layered structure synthesized by hot pressing mixture of TiC_x and Si powder, J. Eur. Ceram. Soc. 32 (12) (2012) 3493–3500.

[32] E. Kaplar, L. Yegorova, K. Lioutov, A. Konobeyev, International Agreement Report "Mechanical Properties of Unirradiated and Irradiated Zr-1% Nb Cladding" NUREG/IA-0199, U.S Nuclear Regulatory Commision, 2001.

[33] Z. Zhao, D. Kunii, T. Abe, H.L. Yang, S. Kano, Y. Matsukawa, et al., Mechanical properties of zircaloy-4 cladding tube by advanced expansion due to compression (A-EDC) test, Mater. Trans. 58 (1) (2016) 46–51.

[34] Status Report on Structural Materials for Advanced Nuclear Systems, NEA No. 6409. 2013.

[35] M. Radovic, M. Barsoum, T. El-Raghy, S. Wiederhorn, W. Luecke, Effect of temperature, strain rate and grain size on the mechanical response of Ti_3SiC_2 in tension, Acta Mater. 50 (6) (2002) 1297–1306.

[36] T. Lapauw, D. Tytko, K. Vanmeensel, S. Huang, P. Choi, D. Raabe, et al., $(Nb_x, Zr_{1-x})_4AlC_3$ max phase solid solutions: processing, mechanical properties, and density functional theory calculations, Inorg. Chem. 55 (11) (2016) 5445–5452.

[37] L. Luzzi, S. Lorenzi, D. Pizzocri, A. Aly, D. Rozzia, A. Del Nevo, Modeling and Analysis of Nuclear Fuel Pin Behavior for Innovative Lead Cooled FBR, ENEA Report, 2014.

[38] Fuel design data, Nucl. Eng. Int. (2004) 26–35 September.

[39] Design, manufacturing and irradiation behaviour of fast reactor fuel, in: Proceedings of the Technical Meeting, IAEA, 2013 IAEA-TECDOC-CD-1689.

[40] W. Huisman, T. Graule, L.W. Huisman, L.J. Gauckler, Centrifugal slip casting of zirconia (TZP), J. Eur. Ceram. Soc. 13 (1) (1994) 33–39.

[41] G.A. Steinlage, R.K. Roeder, K.P. Trumble, K.J. Bowman, Textured ceramic tubes via centrifugal slip casting, Textures Mater. 2 (1996) 1045–1050.

[42] G.A. Steinlage, R.K. Roeder, K.P. Trumble, K.J. Bowman, Centrifugal slip casting of components, Am. Ceram. Soc. Bull. 75 (5) (1996) 92–94.

[43] Y. Katoh, L.L. Snead, C.H. Henager Jr., T. Nozawa, T. Hinoki, A. Iveković, et al., Current status and recent research achievements in SiC/SiC composites, J. Nucl. Mater. 455 (1–3) (2014) 387–397.